RESEARCH PAPER

# Investigation of Tribological Behavior and the Mechanical Properties of TiB₂, Al₂O₃ Reinforced AA6061 Matrix Sintered Hybrid Composites

**Dillibabu Surrya Prakash[1],\*, Narayana Dilip Raja[2]**

*\* dsurryaprakash@gmail.com*

[1]Vel Tech Rangarajan Dr Sagunthala R&D Institute of Science and Technology
[2]Vel Tech Rangarajan Dr Sagunthala R&D Institute of Science and Technology

**Abstract:** *Hybrid composites consisting of AA6061 matrix reinforced with TiB₂ (2, 4, 6, and 8 wt. %), Al₂O₃ (2 wt.%) particles were produced by the sintering process. In comparison to the base material AA6061, the composite produced had improved mechanical properties. The mechanical properties in the sintered composite samples such as tensile strength and hardness, are measured and compared to the wear-tested specimen. Optical micrographs reveal that composites were riddled with defects like blowholes, pinholes, and improper bonding between the particulates before sintering. However, the post-sintered optical micrograph showed that the defects were greatly suppressed. Micrographic images revealed the changes in surface characteristics before and after wear. Until a sliding distance of 260 m, the wear rate of the hybrid composites was kept lower than that of the base material. The coefficient of all the composite materials produced in this study was less than that of the base material. The results reveal that the hardness of hybrid composites having 4 and 6 wt. % of TiB₂ particulates increased by 5.98 and 1.35% respectively. Because of the frictional heating during the wear test, the tensile properties lowered by up to 49.6%. It is concluded that the hybrid composites having 4 and 6 wt. % of TiB₂ particulates exhibited less wear rate for extended sliding distance, good hardness, moderate tensile strength, and decent elongation percentage compared to the base material counterparts.*

**Keywords:** *Hybrid composites, sintering, tensile strength, microhardness, wear, coefficient of friction.*

## 1. INTRODUCTION

Metal Matrix Composites (MMC) comprising of Aluminium alloy AA6061 matrix is preferred for making parts that exhibit characteristics like lightweight, dimensional stability, ductility, corrosion resistance, and high strength [1]. Typical applications of aluminum alloy include automobile parts like bonnet, doors, roofs, and wheels, locomotive body panels, aircraft components, building materials, and sports goods [2]. Mixing the aluminum alloys with reinforcement while making MMC changes the unique characteristics of the alloy. Depending on the composition of the reinforcement added, the alloy can gain or sacrifices a few of its superior properties such as ductility. Adding ceramics as the reinforcement materials enable the aluminum alloy to gain superior tensile strength, hardness, wear resistance, corrosion resistance, and impact strength [3–7]. Adding two or more reinforcements to the matrix is categorized as Hybrid Metal Matrix Composites (HMMC) [8–12].

Casting, powder metallurgy, chemical vapor deposition, and in situ processes are all used to make MMC. The powder metallurgy route is preferred for making MMC and HMMC that has a simple geometry, small size, and dimensional accuracy [13–16]. Sintering process and associated heat transfer benefits in providing superior load-bearing capacity and tribological characteristics extending its applications as automobile brake pads and medical implants [17–20]. Ceramics like Titanium Diboride (TiB₂) and alumina (Al₂O₃) have been used as reinforcement by researchers to determine their influence on the characteristics of the matrix element. It was found that TiB₂ is a stable element in the aluminum alloys even after subjecting the base material to elevated temperature. However, the alloy tends to bond with Ti to become Al3Ti [21]. Mixing Al₂O₃ with Titanium (Ti) in the composition of 1.5 and 3 wt.% revealed increased precipitates formed with elevated temperature during the sintering process [22]. Mixing Al₂O₃ with aluminum alloy developed a stable microstructure, but resulted in inducing brittle properties to the produced MMC [23].

In this study, four different HMMC consisting of varying weight compositions of TiB₂ particulates (2, 4, 6, and 8 wt.%) along with the fixed

composition of $Al_2O_3$ particulates (2 wt.%) were produced by powder metallurgy route. To examine the effect of the reinforcement materials on the matrix element, the mechanical properties and tribological behavior of the HMMCs were compared to the base material AA6061. Microscopic examinations were used to compare the transition in surface properties and also to analyze the defects of the green compact, sintered materials, and the specimen subjected to wear test. The study is aimed at determining the influence of tribological parameters on the mechanical properties of the above-mentioned hybrid laminates.

## 2. EXPERIMENTAL PROCEDURE

### 2.1. Producing the base material and the hybrid composites

The powder metallurgy route is more suitable for adding extremely fine particulates of a nanometric size capable of reducing defects like porosity and improving the mechanical and metallurgical properties of the composites produced [24]. In this study, aluminum alloy AA6061 was chosen as the matrix element of the hybrid composites. An exclusive material without any reinforcement powders was also produced as the base material to act as the reference material. The alloy was produced by mixing 99.7% pure powders (67 μm) of aluminum, chromium, copper, magnesium, ferrous, silicon, and manganese in composition as shown in Table 1. The alloy powders were procured from M/s NR Chem, Mumbai, India. The powders were heated to 135°C in the muffle furnace for 10 mins to remove any moisture present in it [25–28]. The powders were then poured into a glass beaker which was precleaned with acetone and a clean dry cloth. The powders were agitated to evenly disperse and mix the ingredients [4, 29].

**Table 1.** Chemical composition of AA6061

| Material | Weight (%) |
|----------|------------|
| Cr | 0.36 |
| Cu | 0.16 |
| Mg | 0.8 |
| Fe | 0.7 |
| Si | 0.5 |
| Al | Bal. |

The mixed powders were transferred to a mold and subjected to uniaxial compaction at 380

$N/mm^2$ using a 40 Ton Universal Testing Machine (UTM). To minimize the effect of frictional force, lauric acid was used as a lubricant in the die used during compaction [30]. The compaction process was repeated to make four different hybrid composites comprising of varying percentages by weight (2, 4, 6, and 8 wt.%) of the reinforcement powders $TiB_2$ (12~16 μm). The percentage composition of $Al_2O_3$ (37μm) was maintained at 2 wt.% in all the hybrid composites. $TiB_2$ powders were purchased from M/s Nano Research Lab, Jharkhand, India. $Al_2O_3$ powders were supplied by M/s Merck Life Science Pvt., Ltd., Mumbai India.

Table 2 shows the material code relating the percentage composition of the reinforcement powders in the matrix (AA6061). The base material (AA6061) and the respective hybrid composites were compacted in a cast iron die to produce 120 mm long and 20 mm diameter components.

**Table 2.** Composition of produced materials

| Description | Quantity (% by wt.) | | |
|-------------|---------|---------|---------|
| | AA60601 | $TiB_2$ | $Al_2O_3$ |
| Base Material | 100 | - | - |
| Composite A | Bal | 2 | 2 |
| Composite B | Bal | 4 | 2 |
| Composite C | Bal | 6 | 2 |
| Composite D | Bal | 8 | 2 |

The compacted materials were transferred to a vacuum hot press machine with a nitrogen-enriched atmosphere for sintering them. The sintering cycle consisted of heating the compacted powders to 565ºC at a rate of 10ºC/min. The temperature was elevated to 610ºC, where it remained for 60 min. After this duration, the heating was cut-off and the composite or the base material was allowed to cool below 30°C within the furnace.

According to the rule of mixture, the theoretical density was determined as the sum of the densities of individual components in the respective material. The ratio between the mass and volume of the respective materials was used to calculate the green density and sintered density. Surface properties were examined according to ASTM E407 standard using an optical microscope (Make: MEJI. Model: MIL-7100) to compare the microstructures of the pre-sintered and post-sintered composites and the respective base

materials. Scanning Electron Microscope (Make: Hitachi. Model: S3000H. Range: 50X~1000X) equipped with EDAX was used to examine the microstructure of the green compact, sintered material, and also the specimen subjected to wear tests. Fig. 1 and Fig. 2 show the EDAX taken for the base material AA6061 and the hybrid composite A respectively.



**Fig. 1.** EDAX of sintered AA6061



**Fig. 2.** EDAX of hybrid composite A

Wear tests were made on the produced materials using a variable drive pin on the disc machine. The size of the disc was 55 mm in diameter, while the pin (specimen) had a diameter of 10 mm. A supporting weight of 30 N was employed to balance the load transferred through the test specimen [31, 32]. The steel disc was engineered to rotate at 1800 rpm continuously, resulting in a transverse feed of 2 m/s. For each of the developed materials, the wear rate and coefficient of friction were reported. Tensile strength, percentage of elongation, and hardness of the base material and hybrid composites were also evaluated.

The tensile test was carried at 30°C using ASTM E8M-04 standards as shown in Fig. 3. The test specimen was held between the jaws of the ZWICK testing machine and allowing the cross-ram to traverse at $6 \times 10^{-4}$ min$^{-1}$. Hardness was measured in the produced materials using a Vickers hardness test machine (Make: SHIMADZU, Japan; Model: HMV-T1), applying 0.5 kg to the specimen for 15 s. The readings for mechanical properties were taken three times from each specimen.
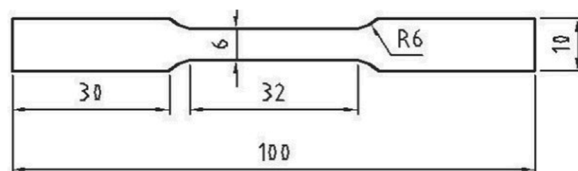


**Fig. 3.** Tensile test specimen dimension [33]

## 3. RESULTS AND DISCUSSION

Fig. 4 shows the comparison between the theoretical density, the density of the green compact, and also that of the sintered materials used in this study. For all the materials, the theoretical density was greater than the green density and sintered density. This occurs because of the entrapment of air within the volume of the compacted materials, causing porosity in the material. The heat supplied during the sintering process enables the removal of air from the green compact, leading to the reduction in the mass of the respective materials.
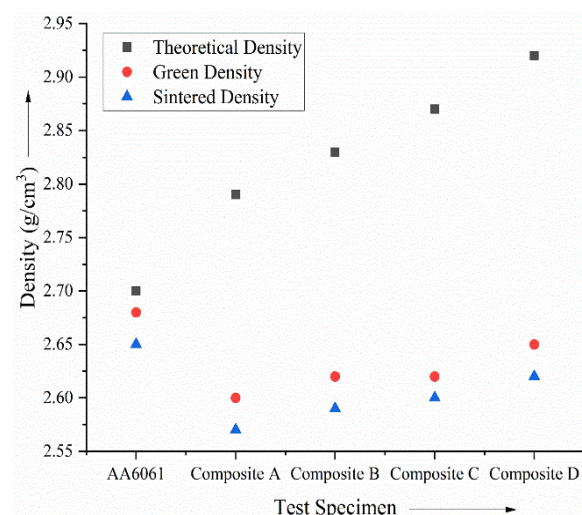


**Fig. 4.** Variation in densities of the produced materials

The reduction of the mass caused the density to decrease. In the base material, AA6061, the deviation from the theoretical density is minimum compared to that of the hybrid composites. It can be inferred that the metal powders used to make the alloy have the same size of 67 μm, facilitating

*Dillibabu Surrya Prakash, Narayana Dilip Raja*

homogeneity during the compaction process. In contrast to the theoretical density, the green density of composite 'A' decreased by 6.81 %, and the sintered density decreased by 7.88 %. The presence of reinforcement particles of 37~45 μm size had a profound effect in increasing the porosity of the hybrid composite.

Theoretically, the density of the hybrid composite increases proportionally with the addition of $TiB_2$ particles. This is because the reinforcement particulates have relatively high density compared to the matrix, which results in increasing the density of the hybrid composites. The densities of the green compact and sintered hybrid composites were lower than those of AA6061, which was surprising. It can be inferred that the large size of the reinforcement particles enabled high porosity during the compaction process entrapping a higher volume of air within the hybrid composites. Subsequently, the removal of air during the sintering of the hybrid composites reduced the mass and lowered its density.

Fig. 5 shows a comparison between the optical microstructure of the produced materials. The compacted specimen of AA6061 had microcavities that originated because of the entrapment of air between the compacted powders and the die head as shown in Fig. 5a. The sintered specimen of AA6061 revealed that the cavities became shallow because of the displacement of plasticized material at elevated temperatures.

The formation of dimpled in the sintered AA6061 reveals that the produced material exhibited ductile behavior as shown in Fig. 5b. Fig. 5c shows that the compacted hybrid composite 'A' had micropores, occurring because of the size variation between the matrix elements and reinforcement powders. Sintered composite 'A' exhibited blow holes that indicate the removal of entrapped air.

The surface of the said composite was riddled with micro chunks of the matrix material indicating that it gained brittle nature as shown in Fig. 5d. Due to the increase in percentage composition of $TiB_2$ particles in the hybrid composite 'B', the size and number of porous holes increased as shown in Fig. 5e. After sintering the hybrid composite 'B', the matrix element AA6061 underwent plastic flow at its surface. However, the surface was riddled with

micropores that occurred while the entrapped air got ejected from the composite as shown in Fig. 5f.

The reinforcement particles agglomerated as the percentage composition of $TiB_2$ particles in the hybrid composite 'C' increased. As a result, the matrix material was clustered into micro islands amidst the agglomerated reinforcement materials as shown in Fig. 5g. After sintering the said hybrid composite, the occurrence of micropores and pinholes is because of the removal of entrapped air from the same as shown in Fig. 5h. Fig. 5i the optical microstructure of the hybrid composite D as reinforcement particulate agglomeration increases.

With the increase in the rienforcement composition, the hybrid composite exhibits tendancy to retain heat energy for prolonged duration. This is because the reinforcement compositions, i.e, 8 wt.% $TiB_2$ and 2 wt.% $Al_2O_3$ particles have low thermal conductivity compared to AA6061. During the syntering process, the hybrid composite was held at elevated temperature for 60 min, which enabled suffecient heating of the reinforcement particulates. After the heater was cut-off, the heat energy was retained for a longer duration. This allowed plastizisation and subsequent precipitation of the matrix element in the hybrid composite as shown in Fig. 5j.

Fig. 6 shows the SEM images of AA6061 before and after sintering. During the green compaction process, the compression of the powders increased the molecular adhesion and cohesion. Because of this, the base material and the composites were able to retain structural integrity. However, the low-grade heat energy impased due to frictional heating during the compaction process had little impact in refining the grain structure of the alloy.

The compressive force during the compaction process was just sufficient to provide structural integrity on the produced material. Some micropores originated due to the mismatch along the edges of the compacted powders as shown in Fig. 5a. During the sintering process, AA6061 underwent grain restructure. However, there was the presence of microcracks and debonding as shown in Fig. 5b. This occurred as the result of heat retention by the alloying composition during the sintering process that deviated from the grain refinement in remote locations.
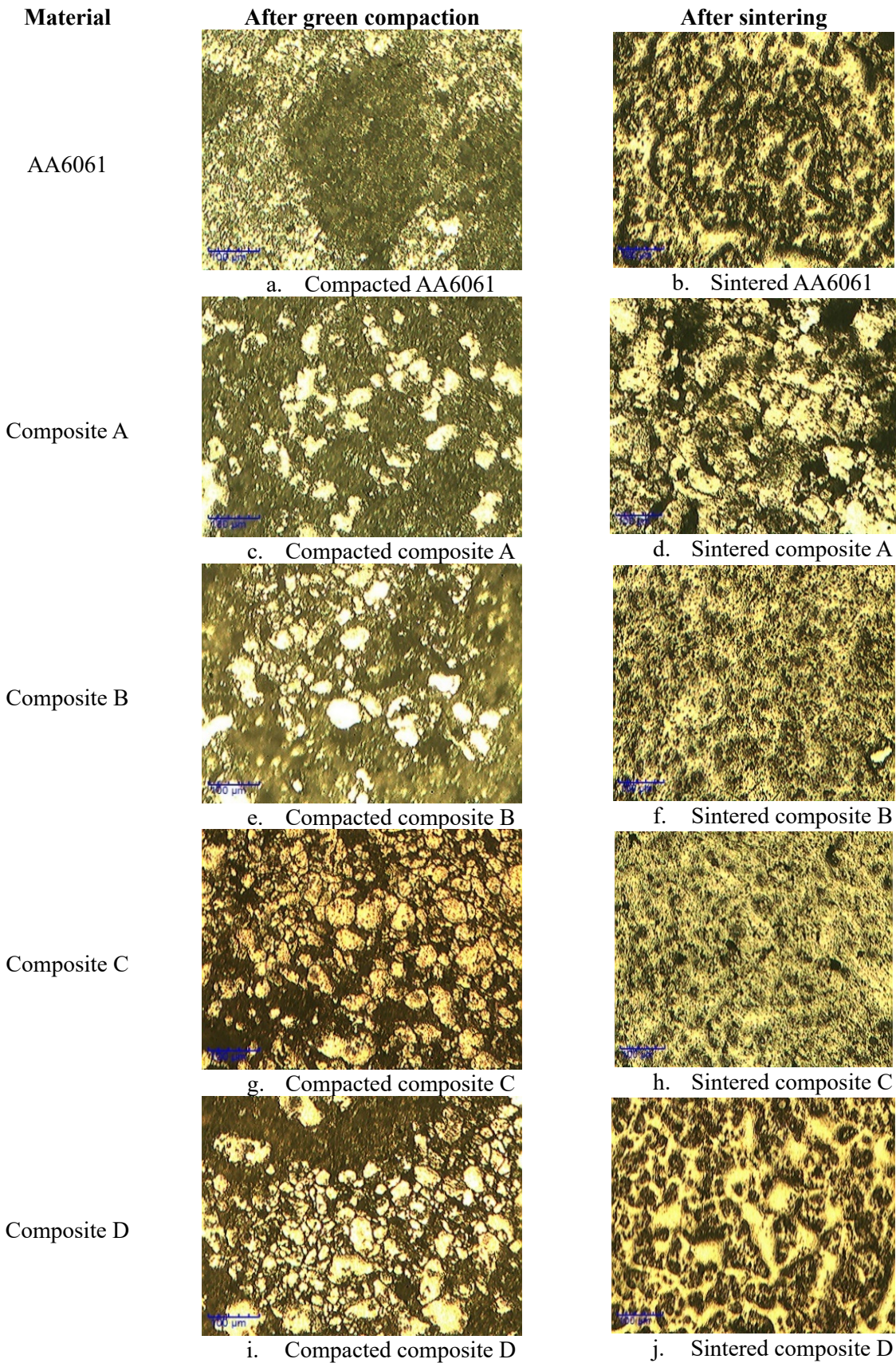
**4**

| Material | After green compaction | After sintering |
|---|---|---|
| AA6061 | a. Compacted AA6061 | b. Sintered AA6061 |
| Composite A | c. Compacted composite A | d. Sintered composite A |
| Composite B | e. Compacted composite B | f. Sintered composite B |
| Composite C | g. Compacted composite C | h. Sintered composite C |
| Composite D | i. Compacted composite D | j. Sintered composite D |

**Fig. 5.** Optical micrographs of the green compact and sintered specimen of AA6061 and hybrid composites

5

*Dillibabu Surrya Prakash, Narayana Dilip Raja*
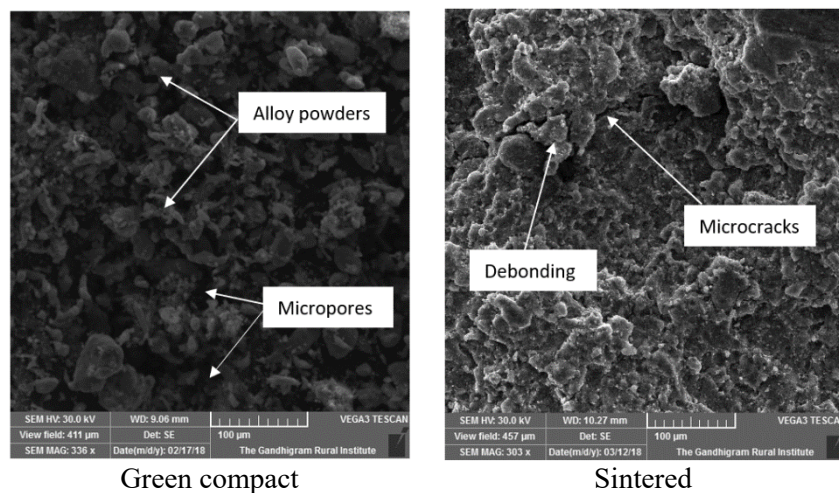
Green compact         Sintered

**Fig. 6.** SEM images of AA6061

Fig. 7 shows the stress vs strain curves of the green compacted materials produced during this study.
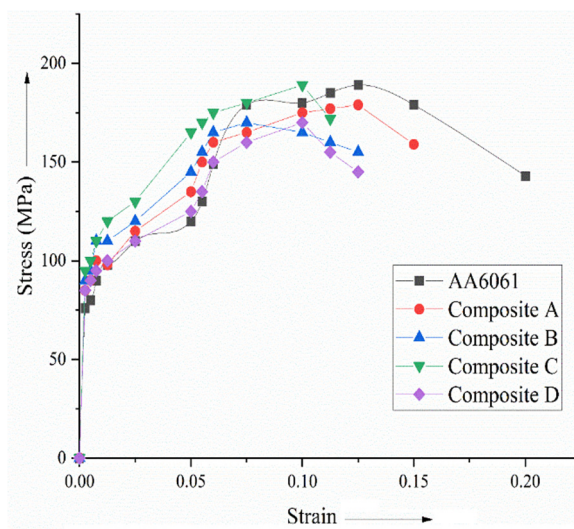


**Fig. 7.** Stress vs Strain

Table 3 shows the parameters recorded during the test. The stress vs strain curve shows that the base material made of AA6061 exhibited characteristics of classic ductile material. The regions of elasticity, transition to plastic deformation, subsequent elongation after reaching the ultimate tensile stress before fracturing under the applied load are evident in the stress strain curve. After adding the reinforcement particles of $TiB_2$ and $Al_2O_3$, the strain exhibited by the composite materials were reduced. It is infered that the adhesion strength of the reinforcement particles with AA6061 during the compaction process was not as strong as the cohesive strength of the matrix material. As the result, the materials disinteragted after attaining their respective ultimate tensile strength.

**Table 3.** Stress and strain parameters of compacted specimen

| Test specimen | Ultimate Tensile strength (MPa) | Fracture strain |
|---|---|---|
| AA6061 | 182 | 0.2 |
| Composite A | 176 | 0.15 |
| Composite B | 172 | 0.12 |
| Composite C | 182 | 0.11 |
| Composite D | 172 | 0.12 |

Interstingly, all materials exhibited similar trends till they reached the ultimate tensile strength, indicating that the compaction process provided suffecient force to increase the strength of cohesion in the matrix element. The variation in stress and strain in the different composites were affected by the strength of adhesion between the reinforcement particles and the matrix element. As the result, the maximum stress and strain of the hybrid composite 'A' were reduced by 5.3 percent and 25%, respectively, when compared to the base material AA6061. Increasing the composition of $TiB_2$ particles by 2 wt.% resulted in the diminishing of the maximum stress and strain of the hybrid composite 'B'. Increasing the $TiB_2$ particle content to 6% increased the maximum stress exhibited by the hybrid composite 'C' to 189 MPa. This was the same as that of the base material at high strain. However, at 8 wt.% of the $TiB_2$ particles the maximum stress value of the hybrid composite 'D' reduced to 170 MPa. It can be inferred that the addition of

6

the two reinforcement particles reduced its ductility.

Fig. 8 shows the extent of wear that occurred on the produced materials concerning the sliding distance. It is observed that for all the materials considered for this study, wear increased with the sliding distance. Surprisingly, up to a sliding distance of 260 m, the wear of all four hybrid composites was lower than that of the base material AA6061. This implies that the reinforcement materials extended their capability to resist wear until a reasonable extent of use. However, the hybrid composite containing 4 wt.% of $TiB_2$ particles and 2 wt.% of $Al_2O_3$ particles exhibited an increase in wear beyond 261 m of sliding distance. High percentage composition of the reinforcement particulates results in low adhesive strength. This leads to debonding of the few particulates over the matrix surface. The loose particulates contribute in grinding the matrix as it gets trapped below the pin of the wear test machine. A lower composition of $TiB_2$ particles i.e., 2 wt.% exhibited lower wear than the base material AA6061 up to 795 m.



**Fig. 8.** Wear vs sliding distance

Contrastingly, the wear of hybrid laminate containing 6 wt. % of $TiB_2$ particles and 2 wt.% of $Al_2O_3$ particles exhibited the lowest wear among all the materials used for this study. Rising the $TiB_2$ particle composition to 8 wt.% reverted the hybrid composite's ability to exhibit an increased wear rate. This is noted by the increase in its wear above the sliding distance of 485 m. It is observed that the trend in wear resistance

exhibited by the hybrid laminate is nonlinear to its reinforcement composition.

It is inferred that composite C, which had superior grain structures when compared to its competitors, had good bonding strength between the matrix and reinforcement materials. This enhanced the ability of the sintered hybrid material, i.e., composite C to distribute the force along the surface subjected to the wear test. Thereby the material was able to withstand the applied force during the wear test and reduce the wear for extended use.

The reason for the increase in the wear rate is attributed to the presence of surface irregularities in the case of composite having 4 wt.% of $TiB_2$ particles. However, in the case of composite having 8 wt.% of $TiB_2$ particles, there was excessive heat dissipation due to constant rubbing of the reinforcement particles. This caused thermal expansion which allowed the detachment of few particulates from the surface. These loose particles increased the abrasion of soft AA6061, leading to an increase in wear.

Fig. 9 shows for all of the materials used in this work, there is a relationship between the coefficient of friction and the sliding distance.
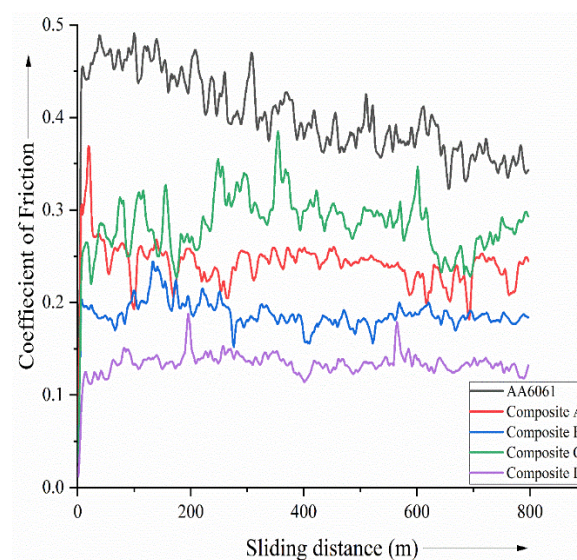


**Fig. 9.** Coefficient of friction vs sliding distance

The base material had the highest coefficient of friction of the four hybrid composites up to a total sliding distance of 800 m. The high coefficient of friction for the base material is because of the high contact area in the absence of reinforcement particulates. It is found that the coefficient of

friction for the composite having 6 wt.% $TiB_2$ particles and 2 wt.% $Al_2O_3$ particles as its reinforcemnets exhibited high coefficient of friction compared among its counterparts.

It can be infered that the reinforcement particulates were intact during the wear test. As the result, the reinforcement particles exhibited high friction over the pin of the wear test machine. The number of reinforcemnt particulates on the surface of the composite material having 2 wt.% and 4 wt.% $TiB_2$ particles along with 2 wt.% $Al_2O_3$ particles were less. Because of less contact area with the pin of the wear test machine, the coefficient of friction recorded during the test was less. However, the high reinforcement particulates in the composite having 8 wt.% $TiB_2$ particles and 2 wt.% $Al_2O_3$ particles resulted in high frictional heat. As the result, the many particulates got detached from the matrix element during the wear test, leading to low coefficient of friction in this composite.

Fig. 10 shows the comparison between the SEM images taken in the produced materials before and after the wear test.
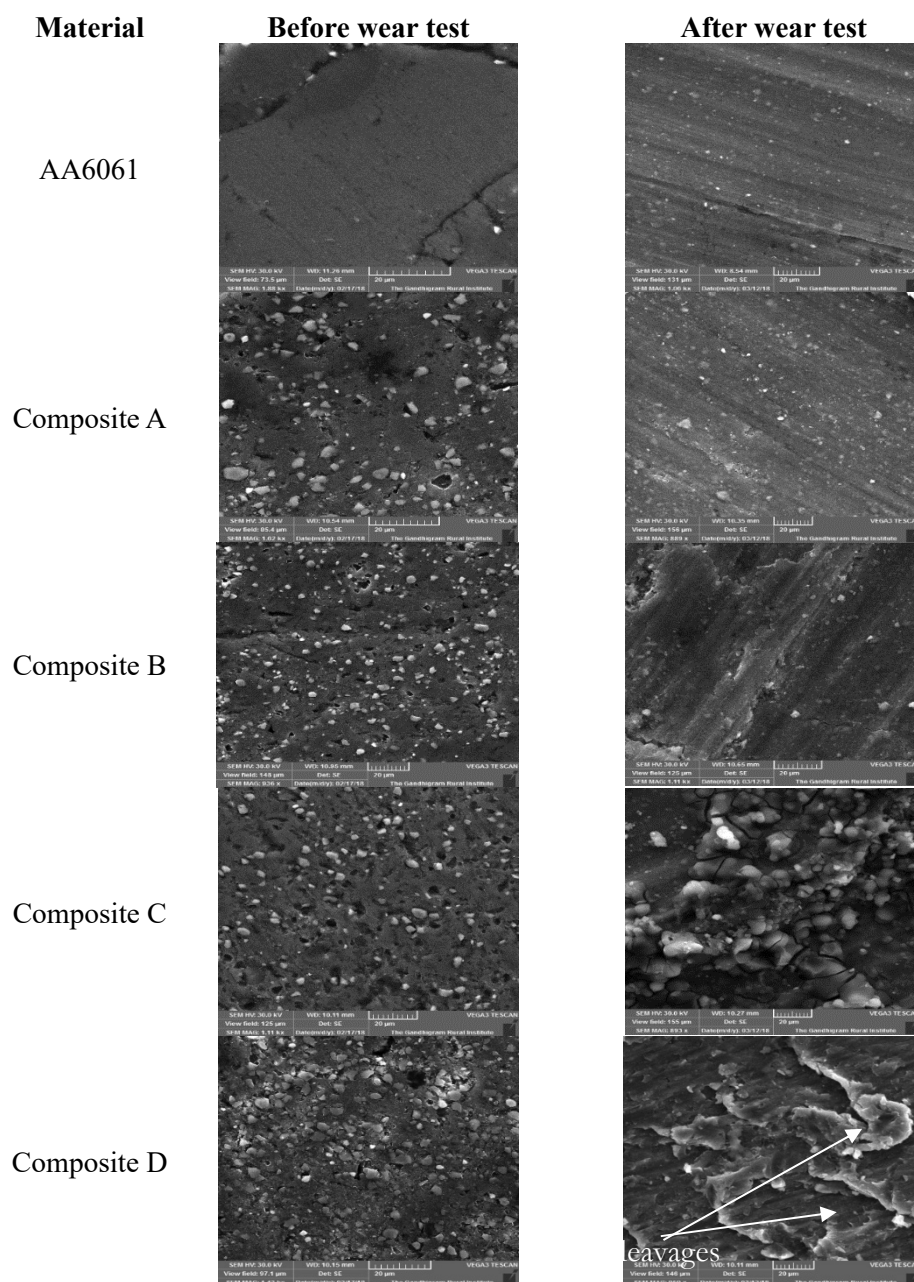


**Fig. 10.** SEM comparison before and after wear test on the produced materials

It is observed that the action of external force on the wear test specimen altered its structural characteristics. Wear lines were clearly distinguished in the base material, hybrid composite A as well as B. The increase in the wear lines indicates that these materials had undergone extensive deformation because of the force from the disc of the wear test machine.

Compared to the base material, hybrid composite A had shallow wear lines, indicating that the presence of the reinforcement particles, 2 wt.% of $TiB_2$ and 2 wt.% of $Al_2O_3$ resisted the extent of wear occurring on the hybrid composite. Increasing the quantity of $TiB_2$ particles to 4 wt.% showed defects like shallow pits and randomly distributed wear lines. This indicates that some of the $TiB_2$ particles got detached because of poor bonding between the matrix and reinforcements in the hybrid composite B. However, the proper bonding between the compositions of hybrid composite C is noted in the SEM image. The retainment of the reinforcement particles after the wear test justifies the low wear and high coefficient of friction in the hybrid composite. In the case of hybrid composite D, defects before the wear test contributed to increasing the wear and lowering the coefficient of friction.

Further, it is noted that the brittle mode of fracture occurred in the wear test hybrid composite D. This is justified by the presence of cleavages in the SEM taken after the wear test. The fracture occurred because of the agglomeration of the reinforcement particulates observed in the sintered hybrid composite D.

Fig. 11 shows the variation in the hardness of the wear-tested hybrid laminates and the base material compared with its counterparts before the wear test. The hardness of the sintered materials before the wear test increased proportionally with the percentage composition of the reinforcements added to the matrix. However, a different scenario was observed after the wear test.

In the case of the base material and the hybrid composite A, the hardness decreased by 6.83% and 4.19% respectively. The frictional heat that occurred during the wear test had changed the surface properties of the material. This is evident from the SEM images shown in Fig. 10. The base material became soft, while the presence of 2 wt.% of each reinforcement particulates reduced the sintered hardness.
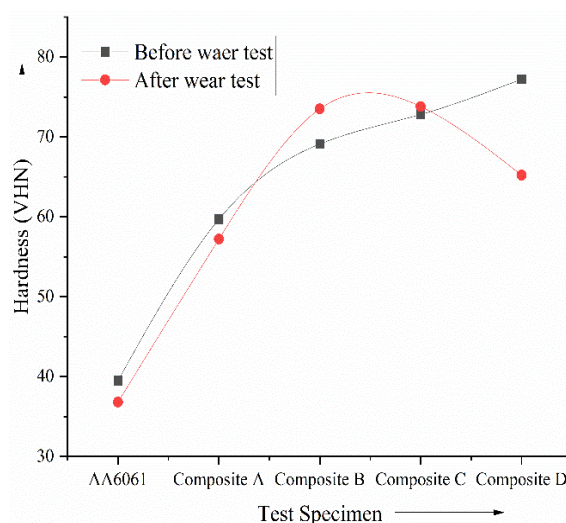


**Fig. 11.** Hardness comparison before and after wear test on the produced materials

However further increase in the percentage composition of $TiB_2$ particles resulted in raising the hardness by 5.98% and 1.35% respectively. This implies that the increase in the percentage composition of the $TiB_2$ particles interfered in the frictional heat transfer and increased the hardness of the sintered hybrid composites. However, increasing the composition of TiB2 particles to 8 wt.% reduced the hardness by 15.54% respectively compared to its counterpart before the wear test. This shows the percentage composition below 4 wt.% and 6 wt.% of the $TiB_2$ particles is determinantal to the hardness of the hybrid composites after subjecting to wear.

The wear test for each specimen was carriedout for a sliding distance of 800 m within 180 min. The corresponding frictional heating of the test specimen resulted in increasing internal heat generation. Since the base material contained only AA6061, the heat energy was dissipated evenly through the test specimen. The base material underwent annealing process because of the slow cooling rate, leading to the reduction of its hardness.

In the case of composite materials, the rate of heat generation and heat loss varied with the percentage composition of their reinforcement particulates. The hybrid composite A had relatively low particulate composition. As the result it mimiced the annealing process that occurred in the base material. Subsequent increase in the reinforcement composition in the hybrid composites B and C resulted in concentration of heat energy near the surface. The

low thermal conductivity of the reinforcement particulates in the hybrid composites resulted in accumulation of heat energy near the surface. Throughout the duration of the wear test, the heat generation was restricted to its surface. After the wear test, the heat energy was quickly dissipated. This lead to increase in the hardness of both the hybrid composites. The reinforcement particulates of composite D debonded from the surface during the wear test. This resulted in heat generation and heat dissipation similar to the base material. As the result, the hardness reduced in the hybrid composite D.

Fig. 12 shows the tensile strength results obtained for the produced materials subjected to the wear test and also before the wear test. It is noted that after the wear test, the base material exhibited a 6.89% increase in tensile strength. This indicates that the frictional heat associated with the wear test altered the properties noted in the sintered material. It is observed that the addition of the reinforcement resulted in reducing the tensile strength by 27.24%, 39.65%, 30.69%, and 12.41% for every 2 wt.% increase in the $TiB_2$ particles.
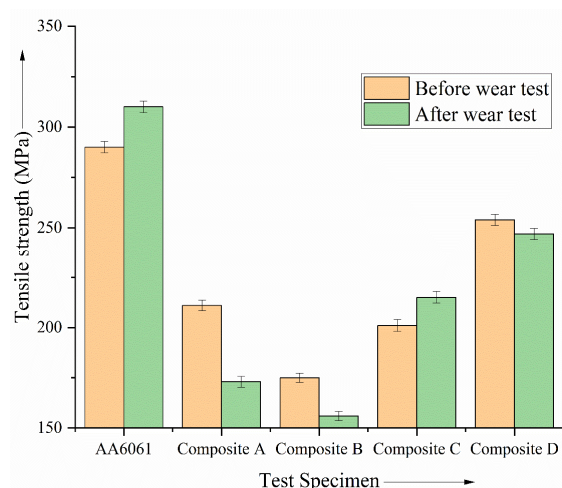


**Fig. 12.** Tensile strength comparison before and after wear test on the produced materials

The influence of $Al_2O_3$ particles is noticed in the rapid depletion in the tensile strength comparing the sintered base material and hybrid composite A. Whereas the influence of $TiB_2$ particles is noted with the non-linear change in the tensile strength which correlated with the quality of the sintered hybrid composites as noted from Fig. 10. This scenario is comparable with the results obtained after the wear test. It is observed that the

frictional heat due to the wear increased the tensile strength by 6.96% because of the superior structural properties of the sintered hybrid composite C. However, for the other three hybrid composites, the tensile strength was reduced after the wear test.

The base material is comprised of the composition of aluminum alloy AA6061, making it homogeneous. As the result, it exhibited isotropic behavior, transmitting the applied load along the volume of the test specimen. However, the addition of $TiB_2$ and $Al_2O_3$ particles converted the resulting hybrid composite to heterogeneous material. Because of this, the hybrid composites attained anisotropic behavior. The applied load increased the internal stress because of the presence of the reinforcement particles distributed within the AA6061 matrix. Hence the base material showed greater tensile strength compared to the hybrid composites.

It is observed that the hybrid composite having less than 6 wt.% of $TiB_2$ particles developed inferior tensile strength. This is because the low composition of the reinforcement particulates induced defects such as micro holes, agglomeration, and microcracks as shown in Fig. 10. These defects contributed to the failure of the hybrid laminates under minimal load. The absence of defects also increased the tensile strength of the base material.

Fig. 13 compares the changes in the elastic properties of the produced materials before and after the wear test. It is noted that the addition of the two reinforcement particles reduced the elastic behavior of the resulting hybrid composites. However, the frictional heat due to the wear increased the tensile property of the base material as noted in Fig. 14. This was because the base material underwent heat treatment that made it ductile. This is justified by the increase in the elongation percentage of the base material. However, the reinforcement materials induced brittle properties to the hybrid composites. Because of this, the elongation of the sintered hybrid composites was reduced and was affected further due to the frictional heat associated with the wear. Hence, the elongation of the wear-tested hybrid composites further reduced by 15.93 %, 6.92%, 12.64%, and 5.88% for the hybrid composite A, B, C, and D respectively.

It is observed that compared between the four hybrid composites, the composite C having

**10**

2 wt.% of Al$_2$O$_3$ particles and 6 wt.% of TiB$_2$ particles exhibited less wear rate for extended sliding distance, good hardness, moderate tensile strength, and decent elongation percentage. Hence the hybrid composite C is taken as a superior material compared to its counterparts.



**Fig. 13.** Elongation properties before and after wear test on the produced materials

## 4. CONCLUSIONS

- Four hybrid composite materials consisting of 2 wt.% of Al$_2$O$_3$ particles and 2, 4, 6, and 8 wt.% of TiB$_2$ particles were produced using powder metallurgy route and sintering process. The mechanical properties such as tensile strength and hardness of the produced hybrid composites were compared with that of the base material AA6061 which was also produced using the powder metallurgy route.
- The sintered hybrid composite sample C consisting of 2 wt.% of Al$_2$O$_3$ particles and 6 wt.% of TiB$_2$ particles exhibited fewer defects than the base materials
- The hybrid composite C exhibited less wear compared to its counterparts and a high coefficient of friction because of proper bonding between the matrix and reinforcement particulates resulting in superior structural rigidity.
- The hardness of the hybrid composite C after the wear test was found to be 1.35% greater than its sintered counterpart. This is because of the grain refinement on the surface of the composite as a result of the frictional heat during the wear test.

- Tensile strength of the hybrid composite C increased after the wear test because of the grain refinement. This enhanced the ability of the sample to distribute load isotropically.
- Percent elongation of hybrid composite C increased by 12.64% compared to its sintered counterpart. However, the mechanical property of the other three hybrid composites was reduced after the wear test.

## REFERENCES

[1] Joel J. and Xavior, M. A., "Aluminium Alloy Composites and its Machinability studies; A Review," Mater. Today Proc., 2018, 5(5), 13556–13562.

[2] Zeid E. F. A., "Mechanical and Electrochemical Characteristics of Solutionized AA 6061, AA6013 and AA 5086 Aluminum Alloys," J. Mater. Res. Technol., 2019, 8(2), 1870–1877.

[3] Zhang, Y., Choudhuri, D., Scharf, T. W., Descartes, S. and Chromik, R. R., "Tribologically Induced Nanolaminate in a Cold-Sprayed WC-Reinforced Cu Matrix Composite: A Key to High Wear Resistance," Mater. Des., 2019, 182, 108-119.

[4] Yang, H., Gao, Y., Frankel, G. S., Qin, W., Li, T., Huang, Z. and Wu, L., "Robust Super hydrophobic Surface with Reinforced Skeletons for Corrosion Protection," Appl. Surf. Sci., 2020, 499, 143-916.

[5] Verma, A. S., Sumankant, Suri, N. M., and Yashpal, "Corrosion Behavior of Aluminum Base Particulate Metal Matrix Composites: A Review," Mater. Today Proc., 2015, 2(4–5), 2840–2851.

[6] Khamei, A. A. and Dehghani, K., "Effects of Strain Rate and Temperature on Hot Tensile Deformation of Severe Plastic Deformed 6061 Aluminum Alloy," Mater. Sci. Eng. A, 2015, 627, 1–9.

[7] Surappa, M. K., "Aluminium matrix composites: Challenges and opportunities," Sadhana - Acad. Proc. Eng. Sci., 2003, 28(1–2), 319–334.

[8] Krishna, M. V. and Xavior, A. M., "An Investigation on the Mechanical Properties of Hybrid Metal Matrix

Composites," Procedia Eng., 2014, 97, 918–92.

[9] Nazari, M., Eskandari, H., and Khodabakhshi, F., "Production and Characterization of an Advanced AA6061-Graphene-TiB$_2$ Hybrid Surface Nanocomposite by Multi-Pass Friction Stir Processing," Surf. Coatings Technol., 2019, 377(6), 1–14.

[10] Xavior, M. A. and Kumar, J. P. A., "Machinability of Hybrid Metal Matrix Composite - A Review," Procedia Eng., 2017, 174, 1110–1118.

[11] James, S. J., Venkatesan, K., Kuppan, P. and Ramanujam, R., "Hybrid Aluminium Metal Matrix Composite Reinforced with SiC and TiB$_2$," Procedia Eng., 2014, 97, 1018–1026.

[12] Nanjan, S. and Janakiram, G. M., "Characteristics of A6061/ (Glass Fibre + Al$_2$O$_3$ + SiC + B$_4$C) Reinforced Hybrid Composite Prepared through STIR Casting," Adv. Mater. Sci. Eng., 2019.

[13] Jeevan, V., Rao, C. S. P., Selvaraj, N. and Rao, G. B., "Fabrication and Characterization of AA6082 ZTA Composites by Powder Metallurgy Process," Mater. Today Proc., 2018, 5(1), 254–260.

[14] Kaku, S. M. Y., Khanra, A. K. and M. Davidson, J., "Micro-structural Analysis and Densification Behavior of Al–ZrB$_2$ Powder Metallurgy Composite During Upsetting," Trans. Indian Inst. Met., 2018, 71(7), 1663–1668.

[15] Singh, L. K., Bhadauria, A., Oraon, A. and Laha, T., "Spark Plasma Sintered Al-0.5 Wt% MWCNT Nanocomposite: Effect of Sintering Pressure on the Densification Behavior and Multi-Scale Mechanical Properties," Diam. Relat. Mater., 2019, 91, 144–155..

[16] Irhayyim, S. S., Hammood, H. S. and Abdulhadi, H. A., "Effect of Nano-TiO$_2$ Particles on Mechanical Performance of Al-CNT Matrix Composite," AIMS Mater. Sci., 2019, 6(6), 1124–1134.

[17] Liu, Z., Ge, Y., Zhao, D., Lou, Y., Liu, Y., Wu, Y., Yu, P. and Yu, C., "Ultrasonic Assisted Sintering Using Heat Converted from Mechanical Energy," Metals (Basel)., 2020, 10(7), 1–

11.

[18] Xiao, Y., Yao, P., Zhou, H., Zhang, Z., Gong, T., Zhao, L. and Deng, M., "Investigation on Speed-Load Sensitivity to Tribological Properties of Copper Metal Matrix Composites for Braking Application," Metals (Basel)., 2020, 10(7), 1–16.

[19] Liu, Y., Chen, F., Xu, G., Cui, Y. and Chang, H., "Correlation Between Microstructure and Mechanical Properties of Heat-Treated Ti–6Al–4V with Fe Alloying" Metals (Basel)., 2020, 10(7), 1–15.

[20] Civantos, A., Giner, M., Trueba, P., Lascano, S., Montoya-García, M. J., Arévalo, C., Vázquez, M. Á., Allain, J. P. and Torres, Y., "In Vitro Bone Cell Behavior on Porous Titanium Samples: Influence of Porosity by Loose Sintering and Space Holder Techniques," Metals (Basel)., 2020, 10(5), 1–20.

[21] Suresh, S. and Moorthi, N. S. V., "Aluminium- Titanium Diboride (Al-TiB$_2$) Metal Matrix Composites: Challenges and Opportunities," Procedia Eng., 2012, 38, 89–97.

[22] Gülsoy, H. Ö., Özbey, S., Pazarlioglu, S., Çiftci, M. and Akyurt, H., "Sintering and Mechanical Properties of Titanium Composites Reinforced Nano Sized Al$_2$O$_3$ Particles," Int. J. Mater. Mech. Manuf., 2015, 4(2), 111–114.

[23] Duntu, S. H., Ahmad, I., Islam, M., and Boakye-Yiadom, S., "Effect of Graphene and Zirconia on Microstructure and Tribological Behaviour of Alumina Matrix Nanocomposites," Wear, 2019, 438–439.

[24] Lu, T., Zhou, M., Ren, L., Fan, L., Guo, Y., Qu, X., Zhang, H., Lu, X. and Quan, G., "Effect of Graphene Nanoplatelets Content on the Mechanical and Wear Properties of AZ31 Alloy," Metals (Basel)., 2020, 10(1265), 1–14.

[25] S. Scudino, "Powder metallurgy of Al-based matrix composites reinforced with quasicrystalline particles." Elsevier Ltd., 2018.

[26] Whalen, S., Olszta, M., Roach, C., Darsell, J., Graff, D., Reza-E-Rabby, M., Roosendaal, T., Daye, W., Pelletiers, T.,

Mathaudhu, S. and Overman, N., "High Ductility Aluminum Alloy Made from Powder by Friction Extrusion," Materialia, 2019, 6, 100-260.

[27] Garg, P., Jamwal, A., Kumar, D., Sadasivuni, K. K., Hussain, C. M. and Gupta, P., "Advance Research Progresses in Aluminium Matrix Composites: Manufacturing and Applications," J. Mater. Res. Technol., 2019, 11, 1–16.

[28] Chen, X., Zhao, G., Liu, G., Sun, L., Chen, L. and Zhang, C., "Microstructure Evolution and Mechanical Properties of 2196 Al-Li Alloy in Hot Extrusion Process," J. Mater. Process. Technol., 2020, 275, 116-348.

[29] Sijo, M. T. and Jayadevan, K. R., "Analysis of Stir Cast Aluminium Silicon Carbide Metal Matrix Composite: A Comprehensive Review," Procedia Technol., 2016, 24, 379–385.

[30] Kumar, P. K., Sai, N. V. and Krishna, A. G., "Influence of Sintering Conditions on Microstructure and Mechanical Properties of Alloy 218 Steels by Powder Metallurgy Route," Arab. J. Sci. Eng., 2018, 43(9), 4659–4674..

[31] Song, W. Q., Krauklis, P., Mouritz, A. P. and Bandyopadhyay, S., "The Effect of Thermal Ageing on the abrasive Wear Behaviour of Age-Hardening 2014 Al/SiC and 6061 Al/SiC Composites," Wear, 1995, 185(1–2), 125–130.

[32] Kumar, N. G. S., Ravindranath, V.M. and Shankar, G. S. S., "Mechanical and Wear Behaviour of Aluminium Metal Matrix Hybrid Composites," Procedia Mater. Sci., 2014, 5(1), 908–917.

[33] Esnaola, J. A., Torca, I., Galdos, L. and Garcia, C., "Determination of the Optimum Forming Conditions for Warm Tube Hydroforming of ZM21 Magnesium Alloy," J. Achiev. Mater. Manuf. Eng., 2009, 32(2), 188–195.